frontiers | Frontiers in Soft Matter

ORIGINAL RESEARCH
published: 24 May 2022
doi: 10.3389/frsfm.2022.890415

Oscillatory Structural Forces Across Dispersions of Micelles With Variable Surface Charge

Michael Ludwig[1], *Philipp Ritzert*[1], *Ramsia Geisler*[1,2], *Sylvain Prévost*[3] *and Regine von Klitzing*[1]*

[1]*Soft Matter at Interfaces, Department of Physics, Technische Universität Darmstadt, Darmstadt, Germany,* [2]*Medical Department 2, Hematology/Oncology and Infectious Diseases, University Hospital of Frankfurt, Frankfurt, Germany,* [3]*Large Scale Structures Group, DS/LSS, Institut Laue-Langevin, Grenoble, France*

When two surfaces interact across colloidal dispersions, oscillatory structural forces often arise due to an ordering of colloidal particles. Although this type of forces was intensively studied, the effect of the surface charge of the colloidal particles is still poorly understood. In the present study, the surface charge of colloidal particles is varied by changing the ratio of nonionic (Tween20) and anionic (sodium dodecyl sulfate, SDS) surfactants of micellar dispersions. The same micellar systems were previously characterised with small-angle neutron scattering (SANS) by the authors, revealing that mixed nonionic-anionic surfactant micelles with variable surface charge form. The present paper addresses the ordering phenomena of the micellar systems under confinement. Therefore, forces across these dispersions were measured for varying surface charges and volume fractions of the micelles, using colloidal-probe atomic force microscopy (CP-AFM). The combination of SANS and CP-AFM experiments allows the dispersions structure in bulk and under geometrical confinement to be compared in terms of the characteristic interparticle distance, correlation length, and ordering strength: In bulk and under confinement, the characteristic intermicellar distance increases by introducing surface charges to micelles until the electrostatic repulsion forces the micelles into a specific ordering. There, the characteristic intermicellar distance purely relates to the micelle volume fraction ϕ as $\propto \phi^{-1/3}$. While in dispersions of uncharged micelles the characteristic intermicellar distance is reduced from bulk to confinement, no such compressibility is observed once the micelles are charged. Furthermore, variation of the micelles surface charge has only little effect on the correlation length of the micelles ordering which is mainly governed by hard-sphere interactions, especially in concentrated dispersions. Introducing surface charges, however, enhances the ordering strength (*i.e.,* the amplitude) of oscillatory structural forces due to stronger electrostatic repulsions of the micelles with the equally charged confining surface. This surface-induced effect is not represented in bulk scattering experiments.

Keywords: micellar dispersions, small-angle neutron scattering, structural force, depletion force, direct force measurements, atomic force microscopy

OPEN ACCESS

Edited by:
Thomas Sottmann, University of Stuttgart, Germany

Reviewed by:
Antonio Stocco, UPR22 Institut Charles Sadron (ICS), France
Vasil M. Garamus, Helmholtz Centre for Materials and Coastal Research (HZG), Germany

***Correspondence:**
Regine von Klitzing
klitzing@smi.tu-darmstadt.de

Specialty section:
This article was submitted to Colloids and Emulsions, a section of the journal Frontiers in Soft Matter

Received: *05 March 2022*
Accepted: *21 April 2022*
Published: *24 May 2022*

Citation:
Ludwig M, Ritzert P, Geisler R, Prévost S and von Klitzing R (2022) Oscillatory Structural Forces Across Dispersions of Micelles With Variable Surface Charge. Front. Soft. Matter 2:890415. doi: 10.3389/frsfm.2022.890415

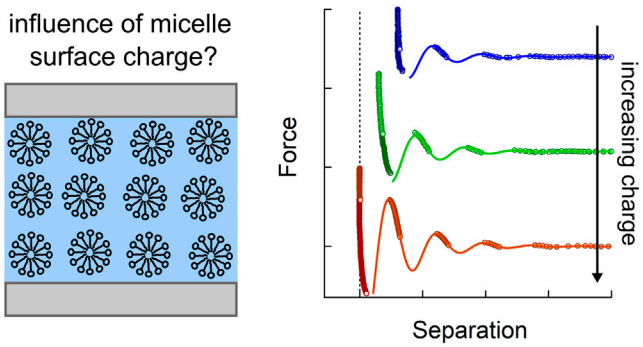

GRAPHICAL ABSTRACT |

1 INTRODUCTION

Oscillatory structural forces are an interesting phenomenon that may arise between two surfaces interacting across colloidal dispersions. Applications in life sciences and engineering often comprise geometrically confined colloidal dispersions in which oscillatory structural forces may be present, such as interacting biomembranes (Kanduč et al., 2017) or surface wetting phenomena (Nikolov and Wasan, 2014). The colloidal particles take a near-ranged ordering in bulk. Close to a macroscopic surface they show an oscillating density profile. When two surfaces approach each other and the oscillating density profiles overlap, the colloidal particles deplete from the forming slit pore between the confining surfaces. Expulsion of particles leads to an osmotic mismatch between the confined region and the bulk reservoir. As a result, an oscillating attractive-repulsive force profile arises upon surface approach. At low particle concentrations only the attractive part, the well-known depletion attraction, occurs (Asakura and Oosawa, 1954; Kralchevsky et al., 2015).

Oscillatory structural forces in dispersions of charged colloidal particles were extensively studied for ionic micelles (Nikolov and Wasan, 1989; Bergeron and Radke, 1992; Richetti and Kékicheff, 1992; McNamee et al., 2004; Tulpar et al., 2006; Tabor et al., 2011a; Tabor et al., 2011b; James and Walz, 2014; Ochoa et al., 2021), polyelectrolytes (Milling and Vincent, 1997; Klitzing et al., 1999; Qu et al., 2006; Biggs, 2010; Üzüm et al., 2011; Browne et al., 2015; Moazzami-Gudarzi et al., 2017; Kubiak et al., 2020), and solid nanoparticles (Piech and Walz, 2002; Piech and Walz, 2004; Drelich et al., 2006; Zeng et al., 2011; Schön and von Klitzing, 2018; Ludwig and von Klitzing, 2021); experimental evidence for oscillatory structural forces in dispersion of uncharged particles is available for aqueous solutions of nonionic surfactants (Basheva et al., 2007; Christov et al., 2010) and latex particles (Basheva et al., 1997; Crocker et al., 1999).

Furthermore, dispersions containing multiple components were investigated. When mixing the uncharged triblock copolymer Pluronic F108 with anionic sodium dodecyl sulfate (SDS) surfactants, both components form complexes that lead to a depletion attraction (Tulpar et al., 2007). Other research reports on the mixing of negatively charged silica nanoparticles with anionic poly (acrylic acid) (PAA) polyelectrolytes (Ji and Walz, 2013), where each component is able to induce oscillatory structural forces on its own. More pronounced oscillatory structural forces occur due to the adsorption of polymers onto the nanoparticles–although both components carry the same charge (Ji and Walz, 2015). Recent work reports on a depletion attraction induced via formation of mixed micelles from nonionic Pluronic P123 triblock-copolymers and SDS (Lele and Tilton, 2020).

Oscillatory structural forces across dispersions containing uncharged particles are theoretically described by statistical mechanics (Henderson, 1988) and density functional theory (Roth et al., 2000). There, the particles interact *via* a hard-sphere potential. These theories led to the development of semiempirical analytical expressions (Kralchevsky and Denkov, 1995; Trokhymchuk et al., 2001) using scaled particle theory (Lebowitz, 1964; Carnahan and Starling, 1969). The expressions derived for hard-sphere interactions do not apply to charged particles because the oscillatory structural force is strongly affected by the long-ranged electrostatic interactions between the particles. The wavelength λ of the force oscillations scales with the particle number density n_p as $\lambda = n_p^{-1/3}$ indicating purely geometrical packing effects. This inverse cubic root scaling law allows to determine the aggregation numbers of various ionic surfactants (Danov et al., 2011; Anachkov et al., 2012) and the diameters of charged solid nanoparticles (Ludwig et al., 2019). The question arises if this scaling law is universal for all charged particles or if it changes with the surface charge of the particles. Recently, (Kralchevsky et al., 2015), reviewed theories of oscillatory structural forces in dispersions of charged and uncharged particles elucidating that the transition point between uncharged and charged particles is still poorly understood, experimentally as well as theoretically.

Charged solid nanoparticles are inappropriate candidates to study the transition point between charged and uncharged particles because their material properties determine the surface charge. Addition of salt or modifications in pH alter the effective surface charge density, but always affecting the background ionic strength. Agglomeration of the charge-

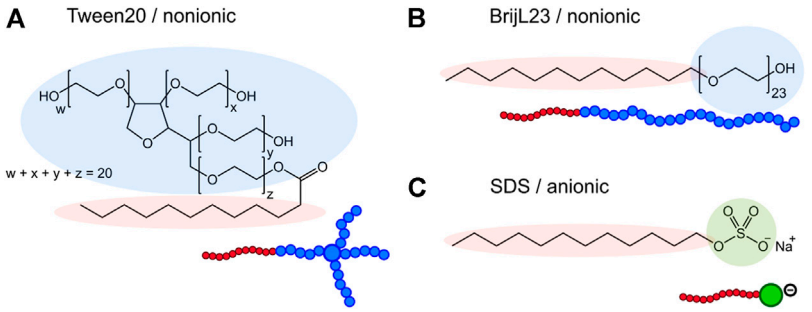

FIGURE 1 | The molecular structures and schematic drawings of the surfactants used in this study: **(A)** nonionic Tween20, **(B)** nonionic BrijL23, and **(C)** anionic SDS. The hydrophobic alkyl chains are highlighted in red. The hydrophilic headgroups are highlighted in blue and green for nonionic EO groups and the anionic sulfate group, respectively. Taken from (Ludwig et al., 2021).

stabilised particles occurs at high ionic strength making it impossible to study uncharged nanoparticles.

To overcome these challenges, the present article systematically studies mixtures of uncharged and charged surfactants at different ratios in the form of self-assembled micelles with variable surface charge. This approach seems particularly promising since the system builds on a known hard-sphere-like fluid and surface charges are subsequently introduced. The main system of interest is composed of the nonionic surfactant Tween20 and the anionic surfactant SDS. Moreover, the well-known nonionic surfactant BrijL23 is investigated to allow comparison with Tween20. Size and shape of individual micelles, the micellar surface charge and bulk ordering in micellar dispersions were previously obtained from small-angle neutron scattering (SANS) experiments (Ludwig et al., 2021). Here, colloidal-probe atomic force microscopy (CP-AFM) probes the oscillatory structural forces across these micellar dispersions. Correlations between the bulk nanostructure and oscillatory structural forces are discussed regarding micellar volume fraction and surface charge of the individual micelles. It is demonstrated how the doping of initially uncharged surfactant micelles enables a precise adjustment of oscillatory structural forces.

2 EXPERIMENTAL SECTION

2.1 Materials

The nonionic surfactants Tween20 (also known as polysorbate 20, **Figure 1A**) and BrijL23 ($C_{12}E_{23}$, previous brand name: Brij-35, **Figure 1B**) were purchased from Sigma Aldrich (Darmstadt, Germany). The anionic surfactant sodium dodecyl sulfate (SDS, ultrapure, **Figure 1C**) was purchased from PanReac AppliChem (Darmstadt, Germany).

Ultrapure water (milliQ-grade, 18.2 MΩ cm resistivity, Merck, Darmstadt, Germany) was used throughout the whole study. All chemicals were used without further purification. Before use, all glassware was cleaned by soaking in aqueous Hellmanex III (Hellma Analytics, Müllheim, Germany) solution for at least 1 h and rinsing with large amounts of water. The mixed surfactant systems were prepared by mixing Tween20 and SDS stock solutions. Four different mixing ratios of SDS and Tween20 were prepared. The mixing ratio X is defined as X = [SDS]/([SDS] + [Tween20]). The composition ranges from X = 0.00 (pure nonionic surfactants) up to X = 0.35 (a proportion of 35 mol% of anionic SDS surfactants). The samples were prepared 3 days before each experiment to allow sufficient dissolution.

2.2 Colloidal Probe Atomic Force Microscopy (CP-AFM)

2.2.1 Substrate and Colloidal Probes

Silicon wafers (Soitec, Bernin, France) were used as substrates. Prior to the experiments, the wafers were cleaned with Piranha solution, using a 1:1 (vol:vol) mixture of hydrogen peroxide (30%, Th. Geyer, Renningen, Germany) and sulphuric acid (96%, Carl Roth, Germany). Afterwards, the wafers were rinsed with large amounts of water and dried in a nitrogen stream. Non-porous silica particles (Bangs Laboratories, Fishers, United States) with a diameter of 5 µm were used as colloidal probes. One particle was glued (UHU Endfest Plus 300, UHU, Bühl, Germany) to the end of a tipless rectangular cantilever (SD-qp-SCONT-TL, Nanosensors, Neuchatel, Switzerland) using a three-dimensional microtranslation stage. Immediately before the experiment, both, cantilever and substrate, were exposed to oxygen plasma (Diener Femto, Ebhausen, Germany) to remove all organic impurities.

2.2.2 Force Measurements

Force measurements were carried out using a Cypher ES atomic force microscope (Asylum Research, Santa Barbara, United States). Before each experiment, the spring constant of the cantilever was determined as 0.012–0.020 N m^{-1} using the method described by (Sader et al., 1999). After calibration, cantilever and substrate were completely immersed into the micellar dispersion. The temperature was set to 20.0°C via a cooler-heater sample stage and left to equilibrate for at least 30 min. The cantilever deflection was measured as a function of the z-piezo position. Using Hooke's law, the cantilever deflection was converted into force. To convert the raw data into force F versus separation h curves (in the following described as force profiles), well-known algorithms are used

(Ducker et al., 1991; Butt et al., 2005; Ralston et al., 2005). The Derjaguin approximation was used to normalise the measured force F against the effective radius R_{eff}. For a planar plate–sphere geometry, R_{eff} is simply the colloidal probe radius R. The resulting force is, therefore, in the following described as $\frac{F}{R}$.

The starting point of each measurement was set to 500 nm with an approach-retraction velocity of typically 50 nm s^{-1}. For very viscous samples (pure Tween20 dispersions at all concentrations and Tween20-SDS mixtures with [c = 146 mM, X = 0.12], [c = 218 mM, X = 0.12], and [c = 224 mM, X = 0.24]), that velocity was reduced to 10 nm s^{-1}. At these velocities, the hydrodynamic force on the cantilever is negligibly small. The surfaces were assumed to be in contact once the normalised force exceeds 0.4 mN m^{-1} (constant compliance region). For each system, at least 30 individual force profile were time averaged (binomial smooth, 10^3 points) to ensure reproducibility and to substantially increase the force resolution.

2.2.3 Fitting of Interaction Forces Between Two Macroscopic Surfaces

The normalised interaction forces $\frac{F}{R}$ between two surfaces at separations h are described by the oscillatory structural force F_{osc}

$$\frac{F}{R}(h) = \frac{F_{\text{osc}}}{R}(h) = -A \cdot \exp\left(-\frac{h}{\xi}\right) \cdot \cos\left(\frac{2\pi}{\lambda}(h - h')\right). \quad (1)$$

with the amplitude A, the decay length ξ, and the wavelength λ. The parameter h' corrects for the offset of the structural force. The fit parameters of the oscillatory structural force may vary so that the fit parameters are not independent of the fit region (Schön and von Klitzing, 2018). To account for this, the starting point of the fit is varied over the stable part of the first force oscillation. Error bars refer to the standard deviations of all individual fits with different starting points in the force profile.

Typically, van der Waals forces are taken into account describing the interaction forces. They are neglected in the following analysis, since they are small and short ranged and do not affect the interactions under the studied conditions. We also neglect double layer forces between the confining surfaces in this study, because they do not influence the force profile at surface separations above the first maximum of the oscillatory force profile.

The surfaces are expected to be in contact at a force of 0.4 mN m^{-1} in order to achieve a stable contact region. In the presence of nonionic surfactants, adsorption of surfactant onto the confining surfaces may occur (Grant et al., 1998). The absolute values of the surface separation h should, therefore, be treated with care.

3 RESULTS AND DISCUSSION

First, the main properties of the micellar dispersions (**Section 3.1**) are revised. Direct force measurements across these dispersions (**Section 3.2**) are then presented. At last, the interplay between bulk nanostructure and oscillatory structural forces is discussed (**Section 3.3**).

The main part contains the analysis of pure Tween20 micelles followed by the investigation of mixed Tween20-SDS micelles. Moreover, pure micellar dispersions of either nonionic BrijL23 or anionic SDS surfactants are investigated for comparison. This analysis can be found as supporting information.

3.1 Bulk Properties of the Micellar Dispersions

The bulk properties of the micellar dispersions were previously studied using small-angle neutron scattering (SANS) (Ludwig et al., 2021). Experimental scattering data, including their analysis, are attached in **Supplementary Figure S1**.

Table 1 summarises the fit results for dispersions of pure Tween20 and mixed Tween20-SDS surfactant micelles. Four different mixing ratios of SDS and Tween20 were investigated. The composition ranges from the pure nonionic Tween20 surfactant (X = 0.00) up to a proportion of 35 mol% of anionic SDS surfactants (X = 0.35). At all mixing ratios X investigated, the nonionic-anionic surfactant mixtures self-assemble into ellipsoidal micelles (**Supplementary Figure S2**) with aspect ratios of 1.36–1.58 (Ludwig et al., 2021). Their effective diameters $2r_{\text{eff}}$ are in the range of 7.50–8.20 nm, a variation of less than 9%. The micelle aggregation number N_{agg} (number of surfactant molecules aggregated in each micelle) decreases slightly with increasing SDS ratio and decreasing volume fraction. The values vary within 15% from pure nonionic micelles to a SDS ratio of X = 0.35. With increasing content of anionic SDS surfactants X, the fractional charge β (number of charges per micelle z divided by the aggregation number N_{agg}) clearly increases up to 21% at a SDS mixing ratio of X = 0.35.

This shows that the approach provides a suitable model system for colloidal dispersions, in which the surface charge of the

TABLE 1 | Properties of mixed Tween20-SDS micelles in bulk dispersions as extracted from SANS measurements. The mixing ratio X is defined as X = [SDS]/([SDS] + [Tween20]). c is the total surfactant concentration ([SDS]+[Tween20]). Parameters obtained from model fitting of SANS data: volume fraction of micelles ϕ, the effective micelles diameter $2r_{\text{eff}}$ (**Supplementary Eq. S1**), the aggregation number N_{agg} (**Supplementary Eq. S2**), and their fractional charge β (**Supplementary Eq. S3**).

X	c / mM	ϕ	$2r_{\text{eff}}$ / nm	N_{agg}	β
0	106	0.190	8.11	94	–
	142	0.240	7.98	95	–
	213	0.333	7.69	92	–
	286	0.374	7.50	101	–
0.12	109	0.215	8.20	88	0.11
	146	0.270	8.09	90	0.10
	218	0.340	7.79	96	0.09
0.24	112	0.200	7.88	87	0.18
	149	0.278	7.97	86	0.16
	224	0.352	7.73	93	0.13
0.35	115	0.202	7.66	81	0.21
	153	0.268	7.70	82	0.20
	230	0.349	7.53	89	0.16

colloidal particles can be gradually changed, while other parameters, such as the particles size remain almost unchanged.

3.2 Oscillatory Structural Forces Across Micellar Dispersions

In this part, the colloidal probe atomic force microscopy (CP-AFM) technique is used to measure forces between two confining surfaces across micellar dispersions. The surfactant concentrations and mixing ratios are the same as used in the former published SANS experiments (**Table 1** and **Supplementary Table S1**). However, contrarily to SANS samples prepared in D_2O, CP-AFM samples are prepared in H_2O. Previous studies on SDS (Chang and Kaler, 1985) and CTAB (Yang and White, 2006; López-Barrón and Wagner, 2011) micelles in solutions of H_2O and D_2O report on isotope effects only at high ionic strength or in liquid crystalline structures. Therefore, no significant change in micellar structure and interactions is assumed or expected in this study.

Forces are measured across pure Tween20 (**Figure 2**), pure BrijL23 (**Supplementary Figure S3**), and pure SDS (**Supplementary Figure S4**) micellar dispersions. The effect of admixing the anionic to nonionic surfactants is demonstrated for Tween20-SDS mixtures (**Figure 3**).

3.2.1 Pure Nonionic Micelles

Figure 2 shows the force profiles between silica surfaces across nonionic Tween20 micellar dispersions measured by CP-AFM.

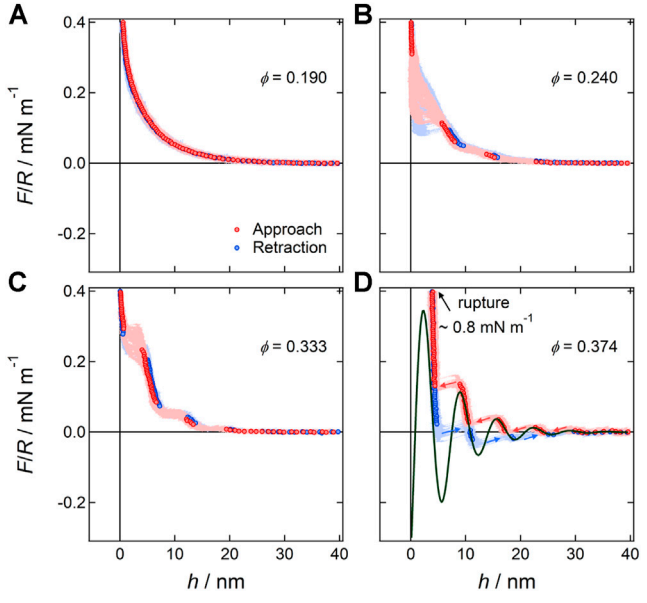

FIGURE 2 | Interaction forces between silica surfaces across nonionic Tween20 micellar dispersions. Red dots are data points for approaching surfaces; blue dots are data points for retracting surfaces. Stacking of all individual data points (bright colours) is shown along with smoothed, time-averaged data (larger dots). Smoothed experimental data are fitted to **Eq. 1** (black, solid line).

All data points of the individual measurements are stacked and displayed in bright colours. This unsmoothed data highlight that the transitions (also referred to as "jumps") between stable force branches are often not clearly pronounced. Jumps in the force profile appear once the gradient in the force profile exceeds the cantilever spring constant. To increase force resolution, the stacked raw data are smoothed and displayed as larger dots (see **Section 2.2.2** for details). Only stable force branches are considered while data point between them are not represented in the smoothed data.

Oscillatory structural forces emerge with increasing volume fraction of Tween20. At a volume fraction of ϕ = 0.240, almost no oscillatory structural forces could be detected which is in agreement with a former study (Christov et al., 2010). At a volume fraction of ϕ = 0.374, clear oscillatory structural forces with at least five oscillations in the force profiles are observed. These experimental data are fitted to a damped oscillatory profile (**Eq. 1**). The high viscosity of the dispersion enhances the thermal noise in the measurement substantially. At surface separations below $h \approx 4.8$ nm, adsorbed surfactant on the silica surfaces may be confined. This layer then ruptures at $\frac{F}{R} \approx 0.8$ mN m^{-1}. The fact that nonionic surfactants can adsorb onto silica surfaces has already been described in literature. Often they form hemicylinders (Grant et al., 1998).

Nonionic BrijL23 micelles show slower formation and decomposition kinetics compared to Tween20 micelles (Patist et al., 2002). BrijL23 micelles are, therefore, considered as more stable. Force profiles across dispersions of BrijL23 micelles are shown in **Supplementary Figure S3**. There, the transitions between stable force branches are more pronounced.

3.2.2 Mixed Nonionic-Anionic Micelles

Interaction forces between silica surfaces across mixed Tween20-SDS micelles are shown in **Figure 3**. The plots are arranged in a manner that: 1) the micelle fractional surface charge β increases from left to right; 2) the volume fraction ϕ increases from top to bottom.

Oscillatory structural forces are observed across all these systems. The magnitude and range varies according to the micelle fractional charge β and volume fraction ϕ. At the smallest volume fraction (ϕ = 0.190) and smallest ratio of anionic surfactants in system (X = 0.12), only one oscillation occurs (**Figure 3A**). The oscillatory structural force becomes stronger due to two reasons: higher micellar surface charge and higher volume fraction. In consequence, the oscillatory structural force is most pronounced in **Figure 3** 1) showing at least four distinct force oscillations up to surface separation above 40 nm.

Additional SDS in the micelles enhances the electrostatic repulsion between individual micelles and also amplifies the interaction between the micelles and the negatively charged confining surfaces. As a result and unlike for pure nonionic Tween20 micelles, no adsorbed surfactant layer is detected. Moreover, the oscillatory structural forces across mixed micellar dispersions are better defined compared to the pure Tween20 micelles, discussed in **Figure 2**.

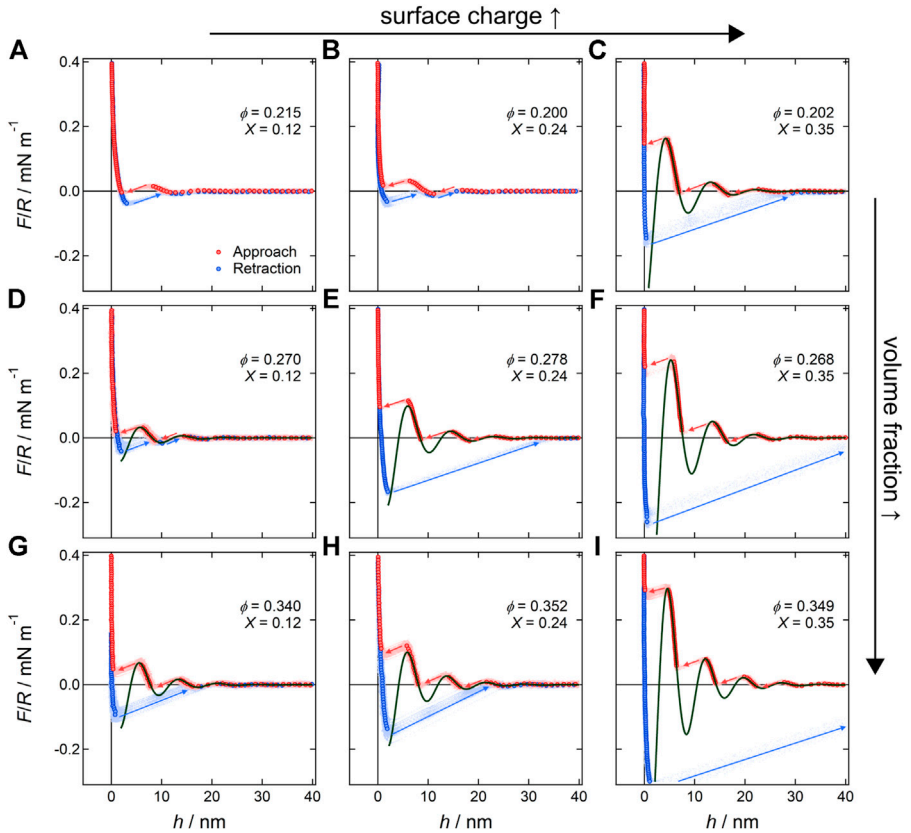

FIGURE 3 | Interaction forces between silica surfaces across mixed Tween20-SDS micellar dispersions for different volume fractions ϕ and different mixing ratios X. Red dots are data points for approaching surfaces, blue dots for retracting surfaces. Stacking of all individual data points (bright colours) is shown along with smoothed, time-averaged data (larger dots). Smoothed experimental data are fitted to **Eq. 1** (black, solid line).

3.3 Comparison of the Bulk Nanostructure and Oscillatory Structural Forces

Further description of the oscillatory structural force involves the discussion of the fit-parameters deduced from **Eq. 1** to the CP-AFM data. These parameters characterise the dispersion structure under geometrical confinement. It is compared to the dispersion bulk structure, as extracted from SANS experiments. Parameters describing the dispersion bulk structure are obtained from a Lorenzian fit to the structure factor $S(q)$ (**Supplementary Eq. S4**). Three different parameters are compared: the characteristic interparticle distance, correlation length, and ordering strength (**Table 2**).

Main focus is on pure Tween20 and mixed Tween20-SDS micellar dispersions. Due to the weakly expressed oscillatory structural forces in **Figures 2A–C**, **3A,D** no fit results can be obtained from these dispersions. The parameters of pure BrijL23 (**Supplementary Figure S6**) and pure SDS (**Supplementary Figure S7**) micellar dispersions are attached as supporting information.

3.3.1 Characteristic Intermicellar Distance

The characteristic intermicellar distances in bulk D^* are extracted from SANS measurements (Ludwig et al., 2021). These values are compared to the characteristic intermicellar distance under confinement extracted as wavelength λ of the oscillatory structural force.

Figure 4 shows the characteristic intermicellar distances obtained in bulk and under confinement as a function of the micelle volume fraction ϕ. Distances are normalised with respect to the effective micelle diameter $2r_{\mathrm{eff}}$ for better comparison.

The characteristic intermicellar distances in bulk $D^*(2r_{\mathrm{eff}})^{-1}$ of uncharged Tween20 micelles vary only little with the volume fraction ϕ (open, black diamonds). At small volume fractions ϕ of uncharged micelles, no pronounced ordering is obtained. The onset of a structure factor $S(q)$ in such systems, however, suggests that some of the micelles are within the pair-potential of neighbouring micelles. As a result, the characteristic intermicellar distance approaches a threshold which is just slightly larger than the diameter of a single micelle (see **Supplementary Figure S5** for more details).

At higher ϕ, the values of nonionic micelles approach the scaling behaviour for charged particles since at close packing geometries ($\phi \approx 0.52$–0.74) the interparticle distances of charged and uncharged particles will not differ. In the same way, it is reasonable that the characteristic distance between micelles at $\phi \approx 0.35$ changes only slightly by introducing surface charges to the micelles. At $\phi \approx 0.20$, the intermicellar distance subsequently increases with increasing ratio of SDS, *i.e.*, with increasing

TABLE 2 | Comparable parameters describing the dispersion structure under confinement and in bulk, extracted from CP-AFM and SANS measurements, respectively.

	Confinement (CP-AFM, Eq. 1)	Bulk (SANS, Supplementary Eq. S4)
Characteristic intermicellar distance	λ	$D^* = \frac{2\pi}{q_{max}}$
Correlation length	ξ	$\frac{2}{\Delta q}$
Ordering strength	A	$S_{max} + S_0 - 1$

fractional surface charge β (indicated by the arrow in **Figure 4**). The electrostatic repulsion between micelles increases with the amount of surface charges. As a result, the micelles form a specific ordering when the micelles exceed a certain amount of surface charge - in this study mixed Tween20-SDS micelles with $X = 0.24$ and $X = 0.35$.

At such an ordering, the characteristic intermicellar distances D^* for charged particles only depends on the particle number density n_p as $D^* \propto n_p^{-1/3}$ considering simple packing arguments. The normalisation to the effective micelle diameter $2r_{\text{eff}}$ transfers this into a dependency on the volume fraction ϕ:

$$\frac{D^*}{2r_{\text{eff}}} = f\,\phi^{-1/3} \tag{2}$$

The type of particle packing determines the value of the pre-factor f. For a simple cubic packing $D^* = n_p^{-1/3} = (4/3\pi)^{1/3} r_{\text{eff}}\,\phi^{-1/3}$, so that $f = 0.806$ in **Eq. 2**. Experimentally $f = 0.718$ is found for the ordering of microemulsion droplets (Lindner and Zemb, 2002). In our study, the charged micelles follow approximately the inverse cubic root scaling law [**Eq. 2** with $f = 0.718$, dashed line in **Figure 4** (mixed Tween20-SDS micelles) and S7 (a) (pure SDS micelles)].

The characteristic interparticle distance in bulk D^* is now compared to the interparticle distance under confinement λ. An existing analytical semiempirical model for the oscillatory structural force exists based on numerical results for hard-sphere fluids to describe the wavelength λ from uncharged micelles. The use of the effective diameter $2r_{\text{eff}}$ again reveals the dependency to the volume fraction ϕ as (Trokhymchuk et al., 2001):

$$\frac{\lambda}{2r_{\text{eff}}} = 2\pi\left(4.45160 + 7.10586\phi - 8.30671\phi^2 + 8.29751\phi^3\right)^{-1} \tag{3}$$

In this study, characteristic intermicellar distance between uncharged Tween20 micelles in bulk (empty black symbols in **Figure 4**) and under confinement (filled black symbol in **Figure 4**) is smaller than predicted by **Eq. 3** (dotted line in **Figure 4**). Interestingly, the bulk intermicellar distance is larger than under confinement ($D^* > \lambda$). The same behaviour is obtained for pure, uncharged BrijL23 micellar dispersions (**Supplementary Figure S6A**). Obviously, uncharged micelles are compressible under confinement. The results from SANS and CP-AFM deviate stronger at higher volume fractions ϕ. In contrast to uncharged micelles, charged micelles obey the same intermicellar distance as in bulk and are not compressible ($D^* = \lambda$). This incompressibility is observed for mixed Tween20-SDS (filled, coloured symbols in **Figure 4**) as well as for pure SDS micellar dispersions (**Supplementary Figure S7A**). The wavelengths λ of all charged micelles are described by their

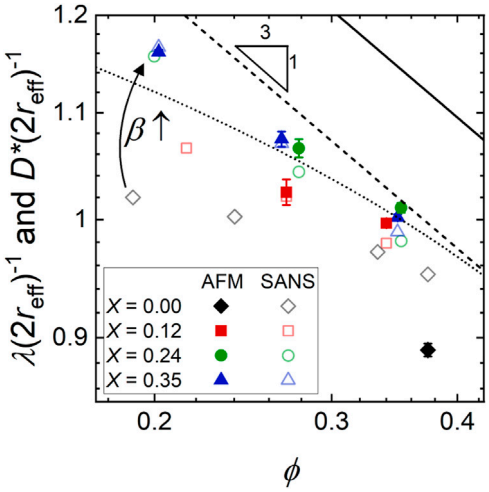

FIGURE 4 | Comparison of the characteristic intermicellar distances: under confinement λ (filled symbols, CP-AFM) and in bulk dispersion D^* (empty symbols, SANS, data from (Ludwig et al., 2021)) as a function of the micelle volume fraction ϕ and for different mixing ratios X, leading to different fractional charges β. Distances are normalised with respect to the effective micelle diameter $2r_{\text{eff}}$. The lines are predictions according to **Eq. 2** with a pre-factor of $f = 0.718$ (dashed line) and $f = 0.806$ (solid line). The dotted line is a prediction according to the theory for uncharged particles (**Eq. 3**).

characteristic intermicellar distance in bulk D^* with $f = 0.718$ (**Eq. 2**). This is in good agreement with a previous study on pure anionic micelles, where $f = 0.698$ is found (Tulpar et al., 2006). Solid colloidal particles, like silica nanoparticles, however, are typically modelled with a factor of $f = 0.806$, indicating perfect simple cubic packing (Tulpar et al., 2006; Zeng and von Klitzing, 2012; Ludwig et al., 2019). The reduction of the intermicellar distances in bulk and under confinements suggests a less pronounced ordering compared to solid colloidal particles. Whether this is due to surfactant micelles being a more dynamic and softer or being more elliptical compared to solid nanoparticles remains unclear.

It has to be further mentioned that the 3D intermicellar structure can only be sensed as 2D representation, both in the SANS and CP-AFM measurements. Therefore, at high volume fractions ($\phi > 0.3$), the characteristic intermicellar distance may be smaller than the effective diameter of the micelle as indicated by a value below 1 of $D^*\,(2r_{\text{eff}})^{-1}$ for uncharged micelles.

3.3.2 Correlation Length

In CP-AFM, the correlation length under confinement is extracted from the decay length ξ from the fit to the

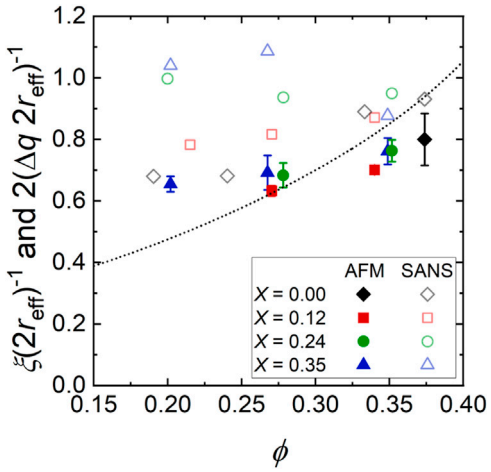

FIGURE 5 | Comparison of the correlation lengths: under confinement as decay length ξ (filled symbols, CP-AFM) and in bulk dispersion as $\frac{2}{\Delta q}$ (empty symbols, SANS, data from (Ludwig et al., 2021)) for all systems studied as a function of their volume fraction ϕ and for different mixing ratios X, leading to different fractional charges β. Distances are normalised to the effective micelle diameter $2r_{\text{eff}}$. The dotted line is a prediction according to the theory for uncharged particles (**Eq. 4**).

oscillatory structural force. In bulk, thus from SANS results, a correlation length is extracted from the full-width at half maximum of the structure peak Δq as $\frac{2}{\Delta q}$.

Figure 5 compares both correlation lengths. The analytical semiempirical model for the oscillatory structural force of uncharged micelles yields the decay length ξ depending on the effective particle radius r_{eff} and the volume fraction ϕ as (Trokhymchuk et al., 2001) (dotted line in **Figure 5**):

$$\frac{\xi}{2r_{\text{eff}}} = \left(4.78366 - 19.64378\phi + 37.37944\phi^2 - 30.59647\phi^3\right)^{-1} \tag{4}$$

In this study, the decay length ξ is almost constant for all dispersions under confinement, irrespective of the micellar surface charge z or volume fraction ϕ. The hard-sphere repulsion is the dominant parameter for the decay length in the confined dispersions and introducing surface charges does not affect these values. The correlation length of the confined dispersions (filled symbols in **Figure 5**) agrees well with the correlation length determined for uncharged micelles in bulk (open, black diamonds in **Figure 5**). The bulk correlation length, however, increases with increasing micellar surface charge. This effect of electrostatic interactions becomes especially important at lower volume fractions, *i.e.,* when the particles are further apart from each other and is only observed between charged micelles in bulk but not under confinement.

3.3.3 Ordering Strength

The amplitude A of oscillatory structural forces is often related to the interparticle interactions in dispersions. It was, however, demonstrated that the interaction between confining surfaces and the particles alters the amplitude A, *e.g.,* by varying the potential of the confining surfaces (Grandner et al., 2009; Grandner and Klapp, 2010; Ludwig and von Klitzing, 2021), meaning that the amplitude does not only depend on properties of the bulk dispersions.

Figure 6 compares the amplitude A with the strength of the intermicellar ordering in bulk calculated from the excess intensity of the structure factor peak: the maximum intensity of the structure factor is normalised to 1: $S_{\text{max}} + S_0 - 1$. This was done, since $S(q) = 1$ indicates a random intermicellar distribution.

The amplitude A of the oscillatory structural forces enhances at higher surface charges of the micelles (**Figure 6A**). The effect of ϕ on A is almost negligible, compared to the influence of the surface charge. The amplitude from the oscillatory structural force across pure Tween20 micelles is neglected in the discussion. There, the first layer in the force profile is considered as an adsorbed layer of nonionic surfactant so

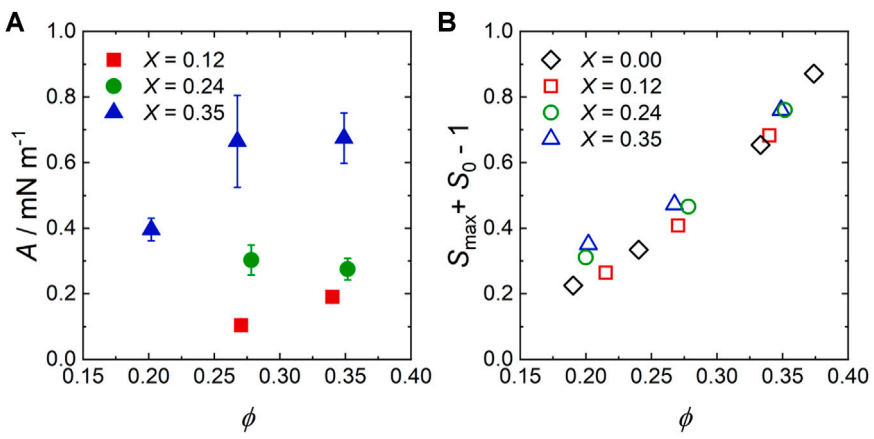

FIGURE 6 | Comparison of **(A)** the amplitude A from CP-AFM force measurements and **(B)** intensity of the structure factor peak $S_{\text{max}} + S_0 - 1$ from SANS measurements (data from (Ludwig et al., 2021)) for all systems studied as a function of their volume fraction ϕ and for different mixing ratios X, leading to different fractional charges β.

that the data cannot be compared. Unlike the effect on A, micellar surface charges do almost not affect the intensity of the structure factor peak $S_{max} + S_0 - 1$ in bulk. This parameter is dominated by the volume fraction ϕ. This means, that ordering of the micelles in bulk is due to hard-sphere repulsions, at $\phi \gtrsim 0.30$. As a result of both values, A and $S_{max} + S_0 - 1$, showing different trends, it is assumed that A strongly depends on the interactions of the micelles with the confining surfaces. This information cannot be obtained from bulk small-angle scattering (SANS) experiments because this parameter does not include any information on the interaction between the micelles and the confining surfaces.

4 CONCLUSION

We have studied the effect of surface charge of colloidal particles on oscillatory structural forces across their respective dispersions with CP-AFM. Since it is impossible to change the surface charge of solid particles without changing other parameters like pH or ionic strength, the study addresses mixed micelles from varying ratios of nonionic (Tween 20) and ionic (SDS) surfactants. The samples investigated range from pure nonionic micelles to micelles containing up to 35% SDS. Under these conditions, self-assembled micelles are of similar size and shape according to former SANS studies. Variation of the mixing ratio adjusts the surface charge. Oscillatory structural forces were successfully measured across these micellar dispersions. The force profile may be well adjusted by a variation of the micellar surface charge as well as the micelle volume fraction.

Comparison of the dispersion properties in bulk and under geometrical confinement reveals different behaviours of uncharged and charged micelles. Charged micelles are forced into a specific ordering by electrostatic repulsion and their characteristic intermicellar distance in bulk $D^\star$ is purely governed by geometrical packing effects and thus scale with the micelle volume fraction ϕ as $D^\star \propto \phi^{-1/3}$. This intermicellar distance does not change from bulk to confinement, as seen in the wavelength λ of the oscillatory structural force ($D^\star = \lambda$), indicating that charged micelles are incompressible during confinement. The bulk intermicellar distance $D^\star$ of uncharged micelles is less sensitive to the micellar number density since the micelles interact only *via* hard-sphere interactions. Furthermore, uncharged micelles can be compressed under geometrical confinement ($D^\star > \lambda$). Differences in the bulk ordering of charged and uncharged micelles become less pronounced at higher volume fractions ($\phi \gtrsim 0.30$) since hard-sphere interactions start to dominate the bulk micellar ordering. Due to this, the micelle surface charge has only little effect on the correlation length of the micelle ordering. Although uncharged and charged micelles show similar bulk ordering at high volume fractions, oscillatory structural forces across these dispersions appear very different because the amplitude of the oscillatory structural force is strongly affected by the interaction of the confining surfaces with the micelles.

In general, this study shows that the inverse cubic root scaling law is not a universal property of all colloidal dispersions. This specific ordering is obtained when the interactions between dispersed particles are highly repulsive. This requirement is only fulfilled for charged particles. When dispersed particles are less charged or even uncharged, their interparticle distance–in bulk as well as under geometrical confinement–is less affected by their volume fraction. These findings might be transferred to various colloidal systems and is not restricted to dispersions of surfactant micelles. This paper might motivate further theoretical studies, since an analytical description of the oscillatory structural force across dispersions of charged particles is still missing.

DATA AVAILABILITY STATEMENT

The original contributions presented in the study are included in the article/**Supplementary Material**, further inquiries can be directed to the corresponding author.

AUTHOR CONTRIBUTIONS

Conceptualization, ML; formal analysis, ML, RG, and SP; investigation, ML and PR; data curation, ML, RG, and SP; resources, RvK; writing-original draft preparation, ML; writing-review and editing, ML, PR, RG, SP, and RvK; supervision, RvK; project administration, RvK; funding acquisition, RvK. All authors have read and agreed to the published version of the manuscript.

ACKNOWLEDGMENTS

The authors thank the Institut Laue-Langevin for the provision of beam time. Data are available from doi:10.5291/ILL-DATA.EASY-440 and doi:10.5291/ILL-DATA.EASY-646. This work benefited from the use of the SasView application, originally developed under NSF award DMR-0520547. SasView contains code developed with funding from the European Union's Horizon 2020 research and innovation programme under the SINE2020 project, grant agreement No. 654000.

SUPPLEMENTARY MATERIAL

The Supplementary Material for this article can be found online at: https://www.frontiersin.org/articles/10.3389/frsfm.2022.890415/full#supplementary-material

REFERENCES

Anachkov, S. E., Danov, K. D., Basheva, E. S., Kralchevsky, P. A., and Ananthapadmanabhan, K. P. (2012). Determination of the Aggregation Number and Charge of Ionic Surfactant Micelles from the Stepwise Thinning of Foam Films. *Adv. colloid interface Sci.* 183-184, 55–67. doi:10.1016/j.cis.2012.08.003

Asakura, S., and Oosawa, F. (1954). On Interaction Between Two Bodies Immersed in a Solution of Macromolecules. *J. Chem. Phys.* 22, 1255–1256. doi:10.1063/1.1740347

Basheva, E. S., Danov, K. D., and Kralchevsky, P. A. (1997). Experimental Study of Particle Structuring in Vertical Stratifying Films from Latex Suspensions. *Langmuir* 13, 4342–4348. doi:10.1021/la970145s

Basheva, E. S., Kralchevsky, P. A., Danov, K. D., Ananthapadmanabhan, K. P., and Lips, A. (2007). The Colloid Structural Forces as a Tool for Particle Characterization and Control of Dispersion Stability. *Phys. Chem. Chem. Phys.* 9, 5183. doi:10.1039/b705758j

Bergeron, V., and Radke, C. J. (1992). Equilibrium Measurements of Oscillatory Disjoining Pressures in Aqueous Foam Films. *Langmuir* 8, 3020–3026. doi:10.1021/la00048a028

Berr, S. S. (1987). Solvent Isotope Effects on Alkytrimethylammonium Bromide Micelles as a Function of Alkyl Chain Length. *J. Phys. Chem.* 91, 4760–4765. doi:10.1021/j100302a024

Biggs, S. (2010). Direct Measurement of the Depletion Interaction in Binary Solutions of Polyelectrolytes. *Phys. Chem. Chem. Phys.* 12, 4172–4177. doi:10.1039/b924680k

Browne, C., Tabor, R. F., Grieser, F., and Dagastine, R. R. (2015). Direct AFM Force Measurements between Air Bubbles in Aqueous Monodisperse Sodium Poly(Styrene Sulfonate) Solutions. *J. colloid interface Sci.* 451, 69–77. doi:10.1016/j.jcis.2015.03.050

Butt, H.-J., Cappella, B., and Kappl, M. (2005). Force Measurements with the Atomic Force Microscope: Technique, Interpretation and Applications. *Surf. Sci. Rep.* 59, 1–152. doi:10.1016/j.surfrep.2005.08.003

Carnahan, N. F., and Starling, K. E. (1969). Equation of State for Nonattracting Rigid Spheres. *J. Chem. Phys.* 51, 635–636. doi:10.1063/1.1672048

Chang, N. J., and Kaler, E. W. (1985). The Structure of Sodium Dodecyl Sulfate Micelles in Solutions of Water and Deuterium Oxide. *J. Phys. Chem.* 89, 2996–3000. doi:10.1021/j100260a009

Christov, N. C., Danov, K. D., Zeng, Y., Kralchevsky, P. A., and von Klitzing, R. (2010). Oscillatory Structural Forces Due to Nonionic Surfactant Micelles: Data by Colloidal–Probe AFM vs Theory. *Langmuir* 26, 915–923. doi:10.1021/la902397w

Crocker, J. C., Matteo, J. A., Dinsmore, A. D., and Yodh, A. G. (1999). Entropic Attraction and Repulsion in Binary Colloids Probed with a Line Optical Tweezer. *Phys. Rev. Lett.* 82, 4352–4355. doi:10.1103/physrevlett.82.4352

Danov, K. D., Basheva, E. S., Kralchevsky, P. A., Ananthapadmanabhan, K. P., and Lips, A. (2011). The Metastable States of Foam Films Containing Electrically Charged Micelles or Particles: Experiment and Quantitative Interpretation. *Adv. colloid interface Sci.* 168, 50–70. doi:10.1016/j.cis.2011.03.006

Drelich, J., Long, J., Xu, Z., Masliyah, J., Nalaskowski, J., Beauchamp, R., et al. (2006). AFM Colloidal Forces Measured Between Microscopic Probes and Flat Substrates in Nanoparticle Suspensions. *J. colloid interface Sci.* 301, 511–522. doi:10.1016/j.jcis.2006.05.044

Ducker, W. A., Senden, T. J., and Pashley, R. M. (1991). Direct Measurement of Colloidal Forces Using an Atomic Force Microscope. *Nature* 353, 239–241. doi:10.1038/353239a0

Grandner, S., and Klapp, S. H. L. (2010). Surface-Charge-Induced Freezing of Colloidal Suspensions. *Epl* 90, 68004. doi:10.1209/0295-5075/90/68004

Grandner, S., Zeng, Y., Klitzing, R., and Klapp, S. H. L. (2009). Impact of Surface Charges on the Solvation Forces in Confined Colloidal Solutions. *J. Chem. Phys.* 131, 154702. doi:10.1063/1.3246844

Grant, L. M., Tiberg, F., and Ducker, W. A. (1998). Nanometer-Scale Organization of Ethylene Oxide Surfactants on Graphite, Hydrophilic Silica, and Hydrophobic Silica. *J. Phys. Chem. B* 102, 4288–4294. doi:10.1021/jp980266g

Henderson, D. (1988). An Explicit Expression for the Solvent Contribution to the Force between Colloidal Particles Using a Hard Sphere Model. *J. colloid interface Sci.* 121, 486–490. doi:10.1016/0021-9797(88)90450-x

James, G. K., and Walz, J. Y. (2014). Experimental and Theoretical Investigation of the Depletion and Structural Forces Produced by Ionic Micelles. *Colloids Surfaces A Physicochem. Eng. Aspects* 441, 406–419. doi:10.1016/j.colsurfa.2013.09.033

Ji, S., and Walz, J. Y. (2013). Synergistic Effects of Nanoparticles and Polymers on Depletion and Structural Interactions. *Langmuir* 29, 15159–15167. doi:10.1021/la403473g

Ji, S., and Walz, J. Y. (2015). Depletion Forces and Flocculation with Surfactants, Polymers and Particles - Synergistic Effects. *Curr. Opin. Colloid & Interface Sci.* 20, 39–45. doi:10.1016/j.cocis.2014.11.006

Kanduč, M., Schlaich, A., de Vries, A. H., Jouhet, J., Maréchal, E., Demé, B., et al. (2017). Tight Cohesion between Glycolipid Membranes Results from Balanced Water-Headgroup Interactions. *Nat. Commun.* 8, 14899. doi:10.1038/ncomms14899

Klitzing, R. v., Espert, A., Asnacios, A., Hellweg, T., Colin, A., and Langevin, D. (1999). Forces in Foam Films Containing Polyelectrolyte and Surfactant. *Colloids Surfaces A Physicochem. Eng. Aspects* 149, 131–140. doi:10.1016/s0927-7757(98)00307-0

Kotlarchyk, M., and Chen, S. H. (1983). Analysis of Small Angle Neutron Scattering Spectra from Polydisperse Interacting Colloids. *J. Chem. Phys.* 79, 2461–2469. doi:10.1063/1.446055

Kralchevsky, P. A., Danov, K. D., and Anachkov, S. E. (2015). Depletion Forces in Thin Liquid Films Due to Nonionic and Ionic Surfactant Micelles. *Curr. Opin. Colloid & Interface Sci.* 20, 11–18. doi:10.1016/j.cocis.2014.11.010

Kralchevsky, P. A., and Denkov, N. D. (1995). Analytical Expression for the Oscillatory Structural Surface Force. *Chem. Phys. Lett.* 240, 385–392. doi:10.1016/0009-2614(95)00539-g

Kubiak, K., Maroni, P., Trefalt, G., and Borkovec, M. (2020). Oscillatory Structural Forces Between Charged Interfaces in Solutions of Oppositely Charged Polyelectrolytes. *Soft Matter* 16, 9662–9668. doi:10.1039/d0sm01257b

Lebowitz, J. L. (1964). Exact Solution of Generalized Percus-Yevick Equation for a Mixture of Hard Spheres. *Phys. Rev.* 133, A895–A899. doi:10.1103/physrev.133.a895

Lele, B. J., and Tilton, R. D. (2020). Depletion Forces Induced by Mixed Micelles of Nonionic Block Copolymers and Anionic Surfactants. *Langmuir* 36, 10772–10784. doi:10.1021/acs.langmuir.0c01574

Lindner, P., and Zemb, T. (2002). *Neutrons, X-Rays and Light: Scattering Methods Applied to Soft Condensed Matter*. 1st ed. (Amsterdam: Elsevier).

López-Barrón, C. R., and Wagner, N. J. (2011). Solvent Isotope Effect on the Microstructure and Rheology of Cationic Worm-like Micelles Near the Isotropic-Nematic Transition. *Soft Matter* 7, 10856. doi:10.1039/c1sm05878a

Ludwig, M., Geisler, R., Prévost, S., and von Klitzing, R. (2021). Shape and Structure Formation of Mixed Nonionic-Anionic Surfactant Micelles. *Molecules* 26, 4136. doi:10.3390/molecules26144136

Ludwig, M., and von Klitzing, R. (2021). Untangling Superposed Double Layer and Structural Forces across Confined Nanoparticle Suspensions. *Phys. Chem. Chem. Phys.* 59, 2010. doi:10.1039/d0cp05631f

Ludwig, M., Witt, M. U., and von Klitzing, R. (2019). Bridging the Gap between Two Different Scaling Laws for Structuring of Liquids under Geometrical Confinement. *Adv. colloid interface Sci.* 269, 270–276. doi:10.1016/j.cis.2019.04.012

McNamee, C. E., Tsujii, Y., Ohshima, H., and Matsumoto, M. (2004). Interaction Forces Between Two Hard Surfaces in Particle-Containing Aqueous Systems. *Langmuir* 20, 1953–1962. doi:10.1021/la0357763

Milling, A. J., and Vincent, B. (1997). Depletion Forces Between Silica Surfaces in Solutions of Poly(acrylic Acid). *Faraday Trans.* 93, 3179–3183. doi:10.1039/a701795b

Moazzami-Gudarzi, M., Maroni, P., Borkovec, M., and Trefalt, G. (2017). Depletion and Double Layer Forces Acting Between Charged Particles in Solutions of Like-Charged Polyelectrolytes and Monovalent Salts. *Soft Matter* 13, 3284–3295. doi:10.1039/c7sm00314e

Nikolov, A. D., and Wasan, D. T. (1989). Ordered Micelle Structuring in Thin Films Formed from Anionic Surfactant Solutions. *J. colloid interface Sci.* 133, 1–12. doi:10.1016/0021-9797(89)90278-6

Nikolov, A., and Wasan, D. (2014). Wetting-Dewetting Films: The Role of Structural Forces. *Adv. colloid interface Sci.* 206, 207–221. doi:10.1016/j.cis.2013.08.005

Ochoa, C., Gao, S., Srivastava, S., and Sharma, V. (2021). Foam Film Stratification Studies Probe Intermicellar Interactions. *Proc. Natl. Acad. Sci.* 118, e2024805118. doi:10.1073/pnas.2024805118

Patist, A., Kanicky, J. R., Shukla, P. K., and Shah, D. O. (2002). Importance of Micellar Kinetics in Relation to Technological Processes. *J. Colloid interface Sci.* 245, 1–15. doi:10.1006/jcis.2001.7955

Piech, M., and Walz, J. Y. (2002). Direct Measurement of Depletion and Structural Forces in Polydisperse, Charged Systems. *J. colloid interface Sci.* 253, 117–129. doi:10.1006/jcis.2002.8503

Piech, M., and Walz, J. Y. (2004). The Structuring of Nonadsorbed Nanoparticles and Polyelectrolyte Chains in the Gap Between a Colloidal Particle and Plate. *J. Phys. Chem. B* 108, 9177–9188. doi:10.1021/jp040067z

Qu, D., Pedersen, J. S., Garnier, S., Laschewsky, A., Möhwald, H., and Klitzing, R. v. (2006). Effect of Polymer Charge and Geometrical Confinement on Ion Distribution and the Structuring in Semidilute Polyelectrolyte Solutions: Comparison between AFM and SAXS. *Macromolecules* 39, 7364–7371. doi:10.1021/ma052676q

Ralston, J., Larson, I., Rutland, M. W., Feiler, A. A., and Kleijn, M. (2005). Atomic Force Microscopy and Direct Surface Force Measurements (IUPAC Technical Report). *Pure Appl. Chem.* 77, 2149–2170. doi:10.1351/pac200577122149

Richetti, P., and Kékicheff, P. (1992). Direct Measurement of Depletion and Structural Forces in a Micellar System. *Phys. Rev. Lett.* 68, 1951–1954. doi:10.1103/physrevlett.68.1951

Roth, R., Evans, R., and Dietrich, S. (2000). Depletion Potential in Hard-Sphere Mixtures: Theory and Applications. *Phys. Rev. E* 62, 5360–5377. doi:10.1103/physreve.62.5360

Sader, J. E., Chon, J. W. M., and Mulvaney, P. (1999). Calibration of Rectangular Atomic Force Microscope Cantilevers. *Rev. Sci. Instrum.* 70, 3967–3969. doi:10.1063/1.1150021

Schön, S., and von Klitzing, R. (2018). A Simple Extension of the Commonly Used Fitting Equation for Oscillatory Structural Forces in Case of Silica Nanoparticle Suspensions. *Beilstein J. Nanotechnol.* 9, 1095–1107. doi:10.3762/bjnano.9.101

Spaar, A., and Salditt, T. (2003). Short Range Order of Hydrocarbon Chains in Fluid Phospholipid Bilayers Studied by X-Ray Diffraction from Highly Oriented Membranes. *Biophysical J.* 85, 1576–1584. doi:10.1016/s0006-3495(03)74589-5

Tabor, R. F., Chan, D. Y. C., Grieser, F., and Dagastine, R. R. (2011a). Structural Forces in Soft Matter Systems. *J. Phys. Chem. Lett.* 2, 434–437. doi:10.1021/jz101574p

Tabor, R. F., Lockie, H., Chan, D. Y. C., Grieser, F., Grillo, I., Mutch, K. J., et al. (2011b). Structural Forces in Soft Matter Systems: Unique Flocculation Pathways between Deformable Droplets. *Soft Matter* 7, 11334. doi:10.1039/c1sm06326j

Trokhymchuk, A., Henderson, D., Nikolov, A., and Wasan, D. T. (2001). A Simple Calculation of Structural and Depletion Forces for Fluids/Suspensions Confined in a Film. *Langmuir* 17, 4940–4947. doi:10.1021/la010047d

Tulpar, A., Tilton, R. D., and Walz, J. Y. (2007). Synergistic Effects of Polymers and Surfactants on Depletion Forces. *Langmuir* 23, 4351–4357. doi:10.1021/la063191d

Tulpar, A., van Tassel, P. R., and Walz, J. Y. (2006). Structuring of Macroions Confined between Like-Charged Surfaces. *Langmuir* 22, 2876–2883. doi:10.1021/la0530485

Üzüm, C., Christau, S., and von Klitzing, R. (2011). Structuring of Polyelectrolyte (NaPSS) Solutions in Bulk and under Confinement as a Function of Concentration and Molecular Weight. *Macromolecules* 44, 7782–7791. doi:10.1021/ma201466a

Yang, B., and White, J. W. (2006). Isotope Effects on the Phase Behaviour of Cetyltrimethylammonium Bromide in H_2O and D_2O Studied by Time Resolved X-Ray Diffraction. *Colloids Surfaces A Physicochem. Eng. Aspects* 277, 171–176. doi:10.1016/j.colsurfa.2005.11.058

Zeng, Y., Grandner, S., Oliveira, C. L. P., Thünemann, A. F., Paris, O., Pedersen, J. S., et al. (2011). Effect of Particle Size and Debye Length on Order Parameters of Colloidal Silica Suspensions under Confinement. *Soft Matter* 7, 10899. doi:10.1039/c1sm05971h

Zeng, Y., and von Klitzing, R. (2012). Scaling of Layer Spacing of Charged Particles under Slit-Pore Confinement: an Effect of Concentration or of Effective Particle Diameter? *J. Phys. Condens. Matter* 24, 464125. doi:10.1088/0953-8984/24/46/464125

Conflict of Interest: The authors declare that the research was conducted in the absence of any commercial or financial relationships that could be construed as a potential conflict of interest.

Publisher's Note: All claims expressed in this article are solely those of the authors and do not necessarily represent those of their affiliated organizations or those of the publisher, the editors, and the reviewers. Any product that may be evaluated in this article, or claim that may be made by its manufacturer, is not guaranteed or endorsed by the publisher.